Connectivity reflects Coding: A Model of Voltage-based Spike-Timing-Dependent-Plasticity with Homeostasis

Claudia Clopath, Lars Büsing*, Eleni Vasilaki, Wulfram Gerstner

Laboratory of Computational Neuroscience

Brain-Mind Institute and School of Computer and Communication Sciences

Ecole Polytechnique Fédérale de Lausanne

1015 Lausanne EPFL, Switzerland

* permanent address: Institut für Grundlagen der Informationsverarbeitung, TU Graz, Austria

June 3, 2009

Abstract

Electrophysiological connectivity patterns in cortex often show a few strong connections in a sea of weak connections. In some brain areas a large fraction of strong connections are bidirectional, in others they are mainly unidirectional. In order to explain these connectivity patterns, we use a model of Spike-Timing-Dependent Plasticity where synaptic changes depend on presynaptic spike arrival and the postsynaptic membrane potential, filtered with two different time constants. The model describes several nonlinear effects in STDP experiments, as well as the voltage dependence of plasticity under voltage clamp and classical paradigms of LTP/LTD induction. We show that in a simulated recurrent network of spiking neurons our plasticity rule leads not only to receptive field development, but also to connectivity patterns that reflect the neural code: for temporal coding paradigms strong connections are predominantly unidirectional, whereas they are bidirectional under rate coding. Thus variable connectivity patterns in the brain could reflect different coding principles across brain areas; moreover our simulations suggest that rewiring the network can be surprisingly fast.

1 Introduction

Experience-dependent changes in receptive fields [1, 2, 3] or in learned behavior [4] may occur through changes in synaptic strength. Thus, electrophysiological measurements of functional connectivity patterns in slices of

neural tissue [5, 6] or anatomical connectivity measures [7] can only present a snapshot of the momentary connectivity – which may change with the next set of stimuli. Indeed, modern imaging methods show that spine motility can lead to a rapid rewiring of the connectivity pattern [8, 9] by formation of new synapses or by strengthening or weakening of existing synapses. The question then arises whether the connectivity patterns and changes that are found in experiments can be connected to basic rules of synaptic plasticity, in particular to modern or traditional forms of Hebbian plasticity [10] such as Long-Term Potentiation and Depression [11].

Long-term potentiation LTP and depression LTD of synapses depends on the exact timing of pre- and postsynaptic action potentials [12, 13], but also on postsynaptic voltage [14, 15], and presynaptic stimulation frequency [16]. Spike-Timing-Dependent Plasticity (STDP) has attracted particular interest in recent years, since temporal coding schemes where information is contained in the exact timing of spikes rather than mean frequency could be learned by a neural system using STDP [17, 18, 19, 20, 21]. The question, however, whether STDP is more fundamental than frequency dependent plasticity or voltage dependent plasticity rules has not been resolved, despite an intense debate [22]. Moreover it is unclear how the interplay of coding and plasticity yield the functional connectivity patterns seen in experiments. In particular, the presence or absence of bidirectional connectivity between cortical pyramidal neurons seems to be contradictory across experimental preparations in visual [5] or somatosensory cortex [6].

Recent experiments have shown that STDP is strongly influenced by postsynaptic voltage before action potential firing [23], but could not answer the question whether spike timing dependence is a direct consequence of voltage dependence, or the manifestation of an independent process. In addition, STDP depends on stimulation frequency [23] suggesting an interaction between timing and frequency dependent processes — or this interaction could be the manifestation of a single process in different experimental paradigms. We show that a simple Hebbian plasticity rule that pairs presynaptic spike arrival with the postsynaptic membrane potential is sufficient to explain STDP and the dependence of plasticity upon presynaptic stimulation frequency. Moreover, the intricate interplay of voltage and spike-timing dependence seen in experiments [23] as well as the frequency dependence of STDP can be explained in our model from one single principle. In contrast of earlier attempts towards a unified description of synaptic plasticity rule that focused on detailed biophysical descriptions [24, 25], our model is a mechanistic one (phenomenological model). It does not give an explicit interpretation in terms of biophysical quantities such a Calcium concentration [24], CaMKII [25], glutamate binding, NMDA receptors etc. Rather it aims at a minimal description of the major phenomena observed in electrophysiology experiments.

The advantage of such a minimal model is that it allows us to discuss functional consequences in small [26, 27], and possibly even large [28, 29], networks. We show that in small networks of up to 10 neurons the learning rule leads to input specificity, necessary for receptive field development - similar to earlier models of STDP [17, 26] or rate-based plasticity rules [30, 31]. Going significantly beyond earlier studies we explicitly address the question of whether functional connectivity patterns of cortical pyramidal neurons measured in recent electrophysiological studies [5, 6] could be the result of plasticity during continued stimulation of neuronal model networks. We found that connectivity patterns strongly depend on the underlying coding hypothesis: With a temporal coding hypothesis, where input spikes arrive in a fixed temporal order, the recurrent network develops a connectivity

pattern with a few strong unidirecitional connections. However, under a rate coding paradigm, where stimuli are stationary during a few hundred milliseconds the same network exhibits sustained and strong bidirectional connections. This is in striking contrast to standard STDP rules where bidirectional connections are impossible [26].

The mathematical simplicity of the model enables us to identify conditions under which it becomes equivalent to the well-known Bienenstock-Cooper-Munro model [30] used in classical rate-based descriptions of developmental learning; and equivalent to some earlier models of STDP [32] — and why our model is fundamentally different from classical STDP models [17, 26, 21], widely used for temporal coding.

2 Results

In order to study how connectivity patterns in cortex can emerge from an interplay of plasticity rules and coding, we need a plasticity rule that is consistent with a large body of experiments, not just a single paradigm such as STDP. Since synaptic depression and potentiation take place through different pathways [33] our model uses separate additive contributions to the plasticity rule, one for LTD and another one for LTP (see Fig. 1 and methods).

2.1 Fitting the Plasticity Model to Experimental Data

Consistent with voltage clamp [15] and stationary depolarization experiments [14] LTD is triggered in our model if presynaptic spike arrival occurs while the membrane potential of the postsynaptic neuron is slightly depolarized (above a threshold θ_{-}) whereas LTP occurs if depolarization is big (above a second threshold θ_{+} (see Fig. 1). The mathematical formulation of the plasticity rule makes a distinction between the momentary voltage u and the low-pass filtered voltage variables \bar{u}_- or \bar{u}_+ which denote temporal averages of the voltage over the recent past (the symbols \bar{u}_{-} and \bar{u}_{+} indicate filtering of u with two different time constants). Similarly, the event x of presynaptic spike arrival needs to be distinguished from the trace $\bar{x}(t)$ that is left at the synapse after stimulation by neurotransmitter. Potentiation occurs only if the momentary voltage is above θ_+ (this condition is fulfilled during action potential firing) AND the average voltage \bar{u}_+ above θ_- (this is fulfilled if there has a been a depolarization in the recent past) AND the trace \bar{x} left by a previous presynaptic spike event is nonzero (this condition holds if a presynaptic spike arrived a few milliseconds earlier at the synapse); these conditions for plasticity are illustrated in Fig. 1B. LTD occurs if the average voltage \bar{u}_{-} is above rest at the moment of a presynaptic spike arrival (see Fig. 1A). The amount of LTD in our model depends on homeostatic process on a slower time scale [34]. Low-pass filtering of the voltage by the variable $(\bar{u}_- \text{ or } \bar{u}_+)$ refers to some unidentified intracellular processes triggered by depolarization, e.g., increase in calcium concentration or second messengers messenger chains. Similarly, the biophysical nature of the trace \bar{x} is irrelevant for the functionality of the model, but a good candidate process is the fraction of glutamate bound to postsynaptic receptors.

We checked the performance of the model on a simulated STDP protocol, where presynaptic spikes arrive

a few milliseconds before or after a postsynaptic spike that is triggered by a strong depolarizing current pulse. If a post-pre pairing with a timing difference of 10 millisecond is repeated 60 times at frequencies below 35Hz, LTD occurs in our model (Fig. 2 A, B), consistent with experiments [23]. Repeated pre-post pairings (with 10 millisecond timing difference) at frequencies above 10Hz yield LTP, but pairings at 0.1Hz do not show any significant change in the model or in experiments [23]. In the model these results can be explained by the fact that at 0.1Hz repetition frequency, the low-pass filtered voltage \bar{u}_+ which increases abruptly during postsynaptic spiking decays back to zero before the next impulse arrives, so that LTP can not be triggered. However, since LTD in the model requires only a weak depolarization of \bar{u}_- at the moment of presynaptic spike arrival, post-pre pairings give rise to depression, even at very low frequency. At repetition frequencies of 50Hz, the post-pre paradigm is nearly indistinguishable from a pre-post timing, and LTP dominates.

Since spike-timing dependence in our model is induced only indirectly via voltage dependence of the model, we wondered whether our model would also be able to account for the intricate interactions of voltage and spike timing found by Sjöström et al. [23]. If a pre-post protocol at 0.1Hz, that normally does not induce LTP, is combined with a depolarizing current pulse (lasting from 50ms before to 50ms after the postsynaptic firing event), then potentiation is observed in the experiments [23], as well as in our model (Fig. 2 C, F, I). Due to the injected current, the low-pass filtered voltage variable \bar{u}_+ is depolarized before the pairing. Thus at the the moment of the postsynaptic spike, the average voltage \bar{u}_+ is above the threshold θ_- leading to potentiation. Similarly, a pre-post protocol that normally leads to LTP can be blocked if the postsynaptic spikes are triggered on the background of a hyperpolarizing current (Fig. 2 E, H, I).

In order to study some nonlinear aspects of STDP, we simulate a protocol of burst-timing-dependent plasticity where presynaptic spikes are paired with 1, 2 or 3 postsynaptic spikes [35] (see Methods). We observe that 60 pre-post pairs at 0.1Hz do not change the synaptic weight, as discussed above. However, repeated triplets pre-post-post generate potentiation in our model because the first postsynaptic spike induces a depolarizing spike after potential so that \bar{u}_+ is depolarized. Adding a third postsynaptic spike to the protocol (i.e., quadruplets pre-post-post-post) does not lead to stronger LTP (Fig. 3A). Our model also describes the dependence of LTP upon the intra-burst frequency (Fig. 3B). At an intra-burst frequency of 20Hz, no LTP occurs, because the second spike in the burst comes so late that the presynaptic trace \bar{x} has decayed back to zero. At higher intra-burst frequencies, the three conditions for LTP $(u(t) > \theta_+$ and $\bar{u}_+ > \theta_-$ and $\bar{x} > 0$) are fulfilled. The burst timing dependence (Fig. 3C) is qualitatively similar to that found in experiments [35], but only four of the six experimental data points are quantitatively reproduced by the model.

2.2 Functional implications

Connectivity patterns in a local cortical circuit have been shown to be non-random, i.e. the majority of connections are weak and the rare strong ones have a high probability of being bidirectional [5]. However, standard models of STDP do not exhibit stable bidirectional connections [36]. Intuitively, if the cell A fires before the cell B, a pre-post pairing for the 'AB' connection is formed so that the connection is strengthened. The post-pre

pairing occurring at the same time in the 'BA' connection leads to depression. Therefore it is impossible to strengthen both connections at the same time. Moreover, in order to assure long-term stability of firing rates parameters in standard STDP rules are typically chosen such that inhibition slightly dominates excitation [17] which implies that under purely random spike firing connections decrease, rather than increase. However, the non-linearity aspects of plasticity in our model change such a simple picture. If we simulate two neurons with bidirectional connections at low firing rates, the plasticity model behaves like standard STDP and only unidirectional connections emerge. However, from Fig. 3B we expect that at higher neuronal firing rates, our model could develop a stable bidirectional connection, in striking contrast to standard STDP rules [21].

Since bidirectional connections require neurons to fire at a high rate, we wondered how coding and connectivity relate to each other. We hypothesized that bidirectional connections are supported by rate-coding as opposed to temporal-coding. To test this idea we first simulated a small network of 10 all-to-all connected neurons in a simplified rate-coding scheme where each neuron fires at a fixed frequency, but the frequency varies across neurons. We find that bidirectional connections are formed only between those neurons that both fire at a high rate, but not if one or both of the neurons fire at low frequencies (Fig. 4A). In a second paradigm, the neurons in the same network are stimulated such that they are firing in a distinct order (1, 2, 3,...) mimicking an extreme form of temporal coding [37]. In that case, the weights form a loop where strong connections from 1 to 2, 2 to 3, ... develop, but no bidirectional connections (Fig. 4B). These results are in striking contrast to simulation experiment with a standard STDP rule, where connections are always unidirectional, independently of coding (Fig. 4C, D).

We wondered whether the same results would emerge in a more realistic network of excitatory and inhibitory neurons driven by feedforward input. We simulated a network of 10 excitatory neurons and 3 inhibitory neurons. Each inhibitory neuron receives input from 8 randomly selected excitatory neurons and randomly projects back to 6 excitatory neurons. In addition to the recurrent input, each excitatory neuron receives feedforward spike input from 500 presynaptic neurons j that generate stochastic Poisson input at a rate ν_j . The rates of neighboring input neurons are correlated, mimicking the presence or absence of spatially extended objects. In a rate-coding scheme, the location of the stimulus is switched every 100ms to a new random position. In case of retinal input, this would correspond to a situation where the subject fixates every 100ms on a new stationary stimulus. In a temporal-coding paradigm, the model input is shifted every 20ms to a neighboring location, mimicking movement of an object across an array of sensory receptors. For both scenarios the network is identical. Feedforward connections and lateral connections between model pyramidal neurons are plastic whereas connections to and from inhibitory neurons are fixed.

After 1000s of stimulation with the rate-coding paradigm, the excitatory neurons developed localized receptive fields and a structured pattern of synaptic connections (Fig. 5B). While the labeling of the excitatory neurons at the beginning of the experiment was randomly assigned, we can relabel the neurons after the formation of lateral connectivity patterns so that neurons with strong reciprocal connections have similar indices, reflecting the neighborhood relation of the network topology. After reordering we can clearly distinguish that three groups of neurons have been formed, characterized by similar receptive fields and strong bidirectional

connectivity within the group, and different receptive fields and no lateral connectivity between groups (Fig. 5C). If the overall amplitude of plastic changes is small (compared to that found in the experiments) the pattern of lateral connectivity is stable and shows a few strong bidirectional connections in a sea of weak lateral connectivity. Unidirectional strong connections are nearly absent. If the amplitude and rate of plasticity is more realistic and in agreement with the data of Fig. 2, then the pattern of lateral connectivity changes between one snapshot and another one 5 seconds later, but the overall pattern is stable when averaged over 100s. In each snapshot, about half of the strong connections are bidirectional (Fig. 5H).

This is in striking contrast with the temporal coding paradigm. Neurons develop receptive fields similar to those seen with the rate-coding paradigm. As expected for temporal Hebbian learning rate [21] the receptive field slowly shifts over time. More importantly, amongst the lateral connections, strong reciprocal links are completely absent (Fig. 6). This suggests that temporal coding paradigms are reflected in the functional connectivity pattern by strong uni-directional connections whereas rate coding leads to strong bidirectional connections.

3 Discussion

Plasticity models over the last decades have primarily focused on questions of development of receptive fields and cortical maps [30], or memory formation [38]. Because traditional plasticity rules are rate models, the relation between coding and connectivity could not be studied. Our plasticity rule is formulated on the level of postsynaptic voltage. Since action potentials present large and narrow voltage peaks, they act as singular events in a voltage rule so that in the presence of spike our rule turns automatically into spike-timing dependent rule. Indeed, for spike coding (and in the absence of significant subthreshold voltage manipulations) our plasticity rule behaves like a STDP rule where triplets of spikes with pre-post-post or post-pre-post timing evoke LTP, whereas pairs with post-pre timing evoke LTD. Moreover, for rate coding where pre- and postsynaptic neurons fire with Poisson firing statistics, our plasticity rule presents structural similarities to the model of Bienenstock, Cooper, and Munro (BCM-model, [30]). Both our spiking rule and the rate-based BCM model require presynaptic activity in order to induce a change. Furthermore for our rule as well as for the simplest BCM rule (see [30]), the depression terms are linear and the potentiation terms are quadratic in the postsynaptic variables (i.e., the postsynaptic potential or the postsynaptic firing rate). Beyond these qualitative similarities, an approximate quantitative relation between the BCM model and our model can be constructed under appropriate assumptions. In this case the total weight change Δw in our model is proportional to $\nu^{\text{pre}}\nu^{\text{post}}(\nu^{\text{post}}-\vartheta)$ where ν^{pre} and $\nu^{\rm post}$ denotes the firing rate of a pre- and postsynaptic neurons, respectively and ϑ is a sliding threshold related to the ratio between the LTP and LTD inducing processes (see methods).

Due to its similarities to BCM, it is not surprising that our spike-based learning rule with sliding threshold is able to support independent component analysis (ICA) that has been hypothesized to underly receptive field development [30, 39]. In our experiments, the input consists of small patches of natural images using standard preprocessing [40]. Image patches are selected randomly and presented to the neuron for T = 200 ms, which

is on the order of a fixation time between saccades [41]. Pixel intensities above an average grey value are converted to spike trains of ON-cells and and those below reference intensity to spikes in OFF-cells, using the relative intensity as the rate of a Poisson process. The spike trains from ON- and OFF-cells are the input to a cortical neuron. The synaptic weights undergo plasticity following our learning rule (Eq. 3). After learning, the weights exhibit a spatial structure that can be interpreted as a receptive field (Fig. 7). In contrast to the principal component analysis of the image patches (as for example implemented by Hebbian learning in linear neurons [42]), the receptive fields are *localized* (i.e. the region with significant weights does not stretch across the whole image patch). Development of localized receptive fields can be interpreted as a signature of ICA [40]. In contrast to most other ICA algorithms [43] our rule is biologically more plausible since it is consistent with a large body of plasticity experiments.

For a comparison of our model with experiments we have mainly focused on experiments in slices of visual cortex, but some of the results can also be related to work in hippocampus. First, as the model explicitly takes into account the postsynaptic membrane potential it can successfully reproduce the voltage dependence of LTP/LTD seen in experiments under depolarization of the postsynaptic membrane [14, 15]. Second, for classical STDP experiments such as [13, 23, 44], which have a stimulation protocol unambiguously defined in terms of preand postsynaptic spike times, the model gives a timing dependence reminiscent of the typical STDP function [13]. Moreover in contrast to standard STDP rules [21], more complicated effects such as the pairing frequency dependence [23] and burst-timing dependence plasticity [35] are qualitatively described. In addition the rule is expected to reproduce the triplet and quadruplet experiments in hippocampal slices [44] (data not shown), because for all STDP protocols the plasticity rule in this paper is similar to an earlier nonlinear STDP rule [32]. Deriving STDP rules from voltage dependence has been attempted before [45, 46]. However, since these earlier models use the momentary voltage [46] or its derivative [45], rather than a combination of momentary and averaged voltage as in our model, these earlier models cannot account for the broad range of nonlinear effects in STDP experiments or interaction of voltage and spike-timing. Our model shows similarities with LTP induction in the TagTriC model [47], but the TagTriC model focuses on the long-term stability of synapses, rather than spike timing dependence of the induction mechanism.

Our plasticity rule allows to explain experiments from two different laboratories by one single principle. Both the "potentiation is rescued by depolarization" [23] scenario (Fig. 2F) and that of burst-timing dependent LTP [35] (Fig. 3) show that LTP at low frequency is induced when the membrane is depolarized before the pre-post pairing. This depolarization can be due to a previous spike during a postsynaptic burst [35] or to a depolarization current. Our model is also consistent with results that LTP can be induced in distal synapses only if additional cooperative input or dendritic depolarization prevent failure of backpropagating action potentials [48]. A further unexpected result is that, with the set of parameters derived from visual cortex slice experiments, synapses fluctuate between strong and weak weights. This aspect is interesting in view of synapse mobility reported in imaging experiment [8].

There are, however, certain limitations to our plasticity rule. First, we did not address the problem of weight dependence of synaptic plasticity and simply assumed that weights can grow to a hard upper bound. Neverthe-

less, the rule can be easily changed to soft bounds [21] by changing the prefactors $A_{\rm LTP}$, $A_{\rm LTD}$ accordingly [47]. Second, short term plasticity [49] could be added for a better description of the plasticity phenomena occurring especially during high frequency protocols. Third, our plasticity rule describes only induction of potentiation or depression during the early phase of LTP/LTD [50]. Additional mechanisms need to be implemented in the model to describe the transition from early to late LTP/LTD [47, 51]. Finally, in modeling voltage-clamp experiments, we assume in our model a unique voltage throughout the whole neuron. In particular the dendrite is assumed to be equipotential to the soma. Yet, experiments controlling the voltage at the soma do not guarantee an equal or even fixed voltage at the synapse with respect to the soma. An obvious and promising improvement would be to use a multi-compartment neuron model (e.g. distinct compartments for the soma and dendrites). In the presented work we did not use a more sophisticated multi-compartment model as this would introduce a considerable number of new parameters making overfitting more likely to occur.

Our plasticity model leads to several predictions that could be tested in slice experiments. First, under the assumption of voltage clamp, our rule is linear in the presynaptic activities (see Methods). Thus the model predicts that in voltage clamp experiments the weight change is only dependent on the voltage and the *number* of presynaptic spikes but not on their exact timing (e.g., low frequency, tetanus, burst input should give the same result). Second, in the scenario where potentiation is rescued by depolarization, the amount of weight change should be the same whether a depolarizing current of amplitude B stops precisely when the postsynaptic spike is triggered or whether a current of slightly bigger amplitude B' stops a few milliseconds earlier. Third, multiple STDP experiments have shown that pre-post pairing (with 10 millisecond timing difference) repeated at 10Hz leads to potentiation [23]. In our plasticity model, LTP occurs in that case because the depolarizing spike-afterpotential of the last postsynaptic spike leads to an increase of the filtered membrane voltage just before the next postsynaptic spike. If this interpretation is correct, a hyperpolarizing current sufficient to cancel the spike afterpotential during 40 milliseconds should block LTP (note that this is different from blocking LTP by a hyperpolarizing current a few milliseconds before the next spike [23]). Alternatively cutting dendrites, i.e. dendrotomy [52] would sharpen the spike after potential.

The influence of STDP on temporal coding has been studied in the past primarily with respect to changes in the feedforward connections [21]. The effect of STDP on lateral connectivity has been studied much less [28, 29, 27]. We have shown in this paper that, because of STDP, coding influences the network topology, because different codes give different patterns of lateral connectivity. Our results are in contrast to standard STDP rules which always suppress short loops, and in particular bidirectional connections [36]. Our more realistic plasticity model shows that under a rate coding paradigm bidirectional connectivity and highly connected clusters with multiple loops are not only possible, but even dominant. It is only for temporal coding, that our biologically plausible rule leads to dominant unilateral directions. Our model also predicts that for a code consisting of synchronous firing events at low frequencies synapses decrease, consistent with earlier findings [27]. We speculate that the differences in coding between different brain areas could lead, even if the learning rule were exactly the same, to different network topologies. Our model predicts that experiments where cells in a recurrent network are repeatedly stimulated in a fixed order would decrease the fraction of strong bidirectional connections, whereas

a stimulation pattern where clusters of neuron fire at high rate during episodes of a few hundred milliseconds would increase this fraction. In this views it is tempting to connect the low degree of bidirectional connectivity in barrel cortex [6] to the bigger importance of temporal structure in whisker input [37], compared to visual input.

4 Acknowledgments

This work has been supported by the European projects FACETS as well as by the Swiss National Science Foundation.

5 Figure Captions

Figure 1: Illustration of the model. Synaptic weights react to presynaptic events (top) and postsynaptic membrane potential (bottom) A. The synaptic weight is decreased if a presynaptic spike x (green) arrives when the low pass filtered value \bar{u}_{-} (magenta) of the membrane potential is above θ_{-} (dashed horizontal line) B. The synaptic weight is increased if the membrane potential u (black) is above a threshold θ^{+} and the low pass filtered value of the membrane potential \bar{u}_{+} (blue) higher than a threshold θ^{-} as well as the presynaptic low pass filter \bar{x} (orange) non zero. C. Step current injection makes the postsynaptic neuron fire at 50Hz in the absence of presynaptic stimulation (membrane potential u in black). No weight change is observed. Note the depolarizing spike-afterpotential consistent with experimental data D., reproduced from [23]. E-H. Voltage clamp experiment. A neuron receives weak presynaptic stimulation of 2Hz during 50s while the postsynaptic voltage is clamped to values between -60mV and 0mV. E-G. Schematic drawing of the trace \bar{x} (orange) of the presynaptic spike train (green) as well as the voltage (black) and the synaptic weight (blue) for the experimental conditions E. Hyperpolarization F. Slight depolarization and G. Large depolarization. H. The weight change as a function of clamped voltage using the standard set of parameters for visual cortex data (blue line, voltage paired with 25 spikes at the synapse). With a different set of parameters the model fits experimental data (red circles) in hippocampal slices [15], see methods for details.

Figure 2: A-B. Simulated STDP experiments. A. Spike-timing dependent learning window. The change of the synaptic weight is shown for different time intervals T between the presynaptic and the postsynaptic spike using 60 presynaptic/postsynaptic spike pairs at 20Hz. B. Weight change as a function of repetition frequency for 5 spike pairs at frequency ρ with a time delay of +10ms (pre-post, blue) and -10ms (post-pre, red), repeated 15 times at 0.1Hz (only 10 times for frequency of ρ =0.1Hz). Weight changes are shown as a function of the frequency, dots represent the data taken from Sjöström et al. [23] and lines the plasticity model simulation. C-I. Interaction of voltage and STDP. C-E. Schematic induction protocols (green: presynaptic input, black: postsynaptic current, blue: evolution of synaptic weight). C. Low-Frequency Potentiation is rescued by depolarization [23]. Low frequency (0.1Hz) pre-post spike pairs yield LTP if a 100ms-long depolarized current is injected around the pairing. D. LTP fails in the previous scenario if an additional brief hyperpolarized pulse is applied 14-ms before postsynaptic spike so that voltage is brought to rest. E. Hyperpolarization preceding action potential prevents potentiation. Sjöström et al. [23] show that high frequency (40Hz) pairing leads to LTP. However, when a constant hyperpolarizing current is applied on top of the short pulses inducing the spikes, no weight change is measured. F. The simulated postsynaptic voltage u (black) following protocol A. is shown as well as the temporal averages \bar{u}_{-} (magenta) and \bar{u}_{+} (blue). The presynaptic spike time is indicated by the green arrow. Using the model Eq. 3 this setting results in potentiation. G. Same as F, but following protocol D. No weight change is measured. H. Same as F., but following protocol E. No weight change is measured. I. Histogram summarizing the normalized synaptic weight of the simulation (bar) and the experimental data [23] (dot, blue bar=variance) 0.1Hz pairing (control 1); 0.1Hz pairing with the depolarization (protocol C.); 0.1Hz pairing with the depolarization and brief hyperpolarization (protocol D.); 40Hz pairing (control 2); 40Hz pairing with the constant hyperpolarization (protocol E.). The parameters are summarized in Table 1B.

Figure 3: Burst-timing-dependent plasticity. One presynaptic spike is paired with a burst of postsynaptic spikes. This pairing is repeated 60 times at 0.1Hz. A. Normalized weight is shown as a function of the number of postsynaptic spikes (1,2,3) at 50Hz. (dots: data from [35], crosses: simulation). The presynaptic spike is paired +10ms before the first postsynaptic spike (blue) or -10ms after (red). B. Normalized weight as a function of the frequency between the three postsynaptic action potentials (dot: data, line: simulation; blue: pre-post, red: post-pre). C. Normalized weight as a function of the timing between the presynaptic spike and the first postsynaptic spike of a 3-spike burst at 50Hz (dot: data, line: simulation). A hard upper bound has been set to 250% normalized weight.

Figure 4: Weight evolution in a all-to-all connected network of 10 neurons. A. Rate code: Neurons fire at different frequencies, neuron 1 at 2Hz, neuron 2 at 4Hz... neuron 10 at 20Hz. The weights (bottom) averaged over 100s show that neurons with high firing rates develop strong bidirectional connections (light blue: weak connections (under 2/3 of the maximal value); yellow: strong unidirectional connections (above 2/3 of the maximal value); brown: strong bidirectional connections). The cluster is schematically represented on top ("after"). B. Temporal code: Neurons fire successively every 20ms (neuron 1 then 20ms later neuron 2, then 3...). Connections (bottom) are unidirectional with strong connections from presynaptic neuron with index n (vertical axis) to postsynaptic neuron with index n+1, n+2 and n+3 leading to a ring-like topology (top: schematic). C. D. Same but with standard STDP rule [17, 26, 21]. Bidirectional connections are impossible.

Figure 5: Plasticity during rate coding. A network of 10 excitatory neurons is connected to 3 inhibitory neurons and receives feedforward inputs from 500 Poisson spike trains with a Gaussian profile of firing rates. The center of the Gaussian is shifted randomly every 100ms A. The schematic figure shows the network before and after the plasticity experiment. B-E. Learning with small amplitudes. Model parameters are taken from table 1B (visual cortex data) except for the amplitudes $A_{\rm LTP}$ and $A_{\rm LTD}$ which are reduced by a factor 100. B. Mean feedforward weights (left) and recurrent excitatory weights (right) averaged over 100s. The grey level graph for the feedforward weights (left) indicates that neurons develop receptive fields that are localized in the input space. The recurrent weights (right) are classified into: light blue - weak (less than 2/3 of the maximal weight), yellow - strong (more than 2/3 of the maximal weight) unidirectional, brown - strong reciprocal connections. The diagonal is white, since self-connections do not exist in the model. C. Same as (B) but for the sake of visual clarity the index of neurons is reordered so that neurons with similar receptive fields have adjacent numbers, highlighting that neurons with similar receptive fields (e.g., neurons 1 to 4) have strong bilateral connections. D. Three snap shots of the recurrent connections taken 5s apart indicating that recurrent connections are stable. E. Histogram of reciprocal, unidirectional and weak connections in the recurrent network averaged over 100s as in (B). The total number of weight fluctuations during 100s is 79 (noted on the figure). The histogram shows an average of 10 repetitions (errorbars are the standard deviation). F-I. Rate code during learning with normal amplitudes. Same network as before but standard set of parameters (table 1B, visual cortex). F. Receptive fields are localized; G. Reordering allows to visualize that the strong bidirectional give rise to clusters of neurons. These clusters are stable when averaged over 100 seconds, but H connections can change from one time step to the next. I. The percentage of reciprocal connections is high, but because of fluctuations (fluc) more than 1000 transitions between strong unidirectional to strong bidirectional or back occur during 100 seconds.

Figure 6: Temporal coding paradigm. The setting is the same as in Fig. 5 (parameters from table 1B, visual cortex) but the input patterns are moved successively every 20ms, corresponding to a step-wise motion of the Gaussian stimulus profile across the input neurons. A. The schematic figure shows the network before and after the plasticity experiment. B. Receptive fields are localized, but in the recurrent network no reciprocal connections appear. C. Reordering of neurons shows that the network develops a ring-like structure with strong unidirectional connections from neuron 8 (vertical axis) to neuron 7 and 6 (horizontal axis); from neuron 7 to neuron 6, 5, and 4; from neuron 4 to neuron 3, 2, and 1 etc. D. Some of the strong unilateral connections appear or disappear from one time step to the next, but the ring-like network structure persists, since the lines just below the diagonal are much more populated than the line above the diagonal. E. Reciprocal connections are completely absent, but unidirectional connections fluctuate several times between 'weak' and 'strong' during 100s.

Figure 7: A small patch of 16x16 pixels is chosen from the whitened natural images benchmark [40]. The patch is selected randomly and is presented as input to 512 neurons for 200ms. The positive part of the image is used as the firing rate to generate Poisson spike trains of the 256 "ON" inputs and the negative one for the 256 "OFF" inputs. B. The weights after convergence are shown for the "ON" inputs and the "OFF" inputs rearranged on a 16x16 image. The filter is calculated by subtracting the "OFF" weights from the "ON" weights. The filter is localized and bimodal, corresponding to an oriented receptive field.

Table 1: A. Parameters for the neuron model. B. Plasticity rule parameters for the various experiments. VC stands for Visual Cortex cells (for experimental details see [23], * standard set of parameters), SC for Somatosensory Cortex cells (see [35]) and HP for Hippocampal cells (see [15]). Bold numbers indicate the free parameters fitted to experimental data. Other parameters are set in advance to values based on the literature.

6 Methods

6.1 Neuron Model

In contrast to standard models of STDP, the plasticity model presented in this paper involves the postsynaptic membrane potential u(t). Hence, predicting the weight change in a given experimental paradigm requires a neuron model that describes the temporal evolution of u(t). For this purpose we chose the adaptive Exponential Integrate-and-Fire (AdEx) model [53] with an additional current describing the depolarizing spike after potential [54]. The neuron model is described by a voltage equation:

$$C\frac{d}{dt}u = -g_L(u - E_L) + g_L\Delta_T \exp\left(\frac{u - V_T}{\Delta_T}\right) - w_{ad} + z + I$$

where C is the membrane capacitance, g_L the leak conductance, E_L the resting potential and I the stimulating current. The exponential term describes the activation of a rapid sodium current. The parameter Δ_T is called the slope factor and V_T the threshold potential [53]. A hyperpolarizing adaptation current is described by the variable w_{ad} with dynamics

$$\tau_{w_{ad}} \frac{d}{dt} w_{ad} = a(u - E_L) - w_{ad},$$

where $\tau_{w_{ad}}$ is the time constant of the adaption of the neuron. Upon firing the variable u is reset to a fixed value V_{reset} whereas w_{ad} is increased by an amount b. The main difference to the Izhikevich model [55] is that

the voltage is exponential rather than quadratic allowing a better fit to data [54]. The spike afterpotential of the cells used in typical STDP experiments [23] have a long depolarizing spike after potential. We therefore add an additional current z which is set to a value I_{sp} immediately after a spike occurs and decays otherwise with a time constant τ_z .

$$\tau_z \frac{d}{dt} z = -z,$$

Finally, refractoriness is shown in pyramidal cells [54] and therefore is modeled with the adaptive threshold V_T . Therefore V_T is set to $V_{T_{max}}$ after a spike and decays to $V_{T_{rest}}$ with a time constant τ_{V_T} as measured in [54], i.e.

$$\tau_{V_T} \frac{d}{dt} V_T = -(V_T - V_{T_{rest}}).$$

Parameters for the neuron model are taken from [53] for the AdEx, τ_z is set to 40ms in agreement with [23, 54] and kept fixed throughout all simulations (see table 1A).

6.2 Plasticity Model

Since synaptic depression and potentiation take place through different pathways [33] our model exhibits separate additive contributions to the plasticity rule, one for LTD and another one for LTP.

For the LTD part, we assume that presynaptic spike arrival at synapse i induces depression of the synaptic weight w_i by an amount $-A_{\rm LTD} [\overline{u}_-(t) - \theta_-]_+$ that is proportional to the average postsynaptic depolarization \overline{u}_- . The brackets $[]_+$ indicate rectification, i.e. any value $\overline{u}_- < \theta_-$ does not lead to a change and implement experimental findings showing that postsynaptic depolarization should exceed a certain value θ^- to establish depression of the synapse [14] (see Fig. 1H). The quantity $\overline{u}_-(t)$ is an exponential low-pass filtered version of the postsynaptic membrane potential u(t) with a time constant τ_- :

$$\tau_{-}\frac{d}{dt}\overline{u}_{-}(t) = -\overline{u}_{-}(t) + u(t).$$

The variable \bar{u}_- is an abstract variable which could, for instance, reflect the level of calcium concentration [24] or the release of endocannabinoids [56], though such an interpretation is not necessary for our rule. Since the presynaptic spike train is described as a series of short pulses at time t_i^n where i is the index of the synapse and n an index that counts the spike, $X_i(t) = \sum_n \delta(t - t_i^n)$, depression is modeled as the following update rule, see also Fig. 1:

$$\frac{d}{dt}w_i^- = -A_{\rm LTD}(\bar{\bar{u}}) X_i(t) [\bar{u}_-(t) - \theta_-]_+ \quad \text{if } w_i > w_{\min},$$
(1)

where $A_{\rm LTD}(\bar{u})$ is an amplitude parameter that is under the control of homeostatic processes [34]. For slice experiment the parameter has a fixed value extracted from experiment. For network simulations, we make it depend on the mean depolarization \bar{u} of the postsynaptic neuron, averaged over a time scale of 1 second. Eq. 1

is a simple method to implement homeostasis; other methods such as weight rescaling would also be possible [34].

For the LTP part, we assume that each presynaptic spike at the synapse w_i increases the trace $\bar{x}_i(t)$ of some biophysical quantity, which decays exponentially with a time constant τ_x in the absence of presynaptic spikes, similar to previous work [17, 32]. The temporal evolution of $\bar{x}_i(t)$ is described by:

$$\tau_x \frac{d}{dt} \bar{x}_i(t) = -\bar{x}_i(t) + X_i(t),$$

where X_i is the spike train defined above. The quantity $\bar{x}_i(t)$ could for example represent the amount of glutamate bound to postsynaptic receptors [32] or the number of NMDA receptors in an activated state. The potentiation of w_i is modeled by the following expression, which is proportional to the trace $\bar{x}_i(t)$ (see also Fig. 1):

$$\frac{d}{dt}w_i^+ = +A_{\text{LTP}}\,\bar{x}_i(t)\,[u(t) - \theta_+]_+\,[\bar{u}_+(t) - \theta_-]_+ \quad \text{if } w_i < w_{\text{max}}.$$
(2)

Here, $A_{\rm LTP}$ is a free amplitude parameter fitted to the data and $\overline{u}_+(t)$ is another low-pass filtered version of u(t) similar to $\overline{u}_-(t)$ but with a shorter time constant τ_+ around 10ms. Thus positive weight changes can occur if the momentary voltage u(t) surpasses a threshold θ_+ and, at the same time the average value $\overline{u}_+(t)$ is above θ_- .

The final rule used in the simulation is described by the equation

$$\frac{d}{dt}w_{i} = -A_{\text{LTD}}(\bar{u}) X_{i}(t) [\bar{u}_{-}(t) - \theta_{-}]_{+} + A_{\text{LTP}} \bar{x}_{i}(t) [u(t) - \theta_{+}]_{+} [\bar{u}_{+}(t) - \theta_{-}]_{+},$$
(3)

combined with hard bounds $0 \le w_i \le w_{max}$. For network simulation, $A_{\text{LTD}}(\bar{\bar{u}}) = A_{\text{LTD}} \frac{\bar{u}^2}{u_{ref}^2}$ where u_{ref}^2 is a reference value.

6.3 Parameters and Data Fitting

For the plasticity experiments in slices, we take $\bar{u} = u_{ref}$ as fixed and fit the parameters $A_{\rm LTD}$. The total number of parameters of the plasticity model is then 7. For all data sets, except the one taken from [15], the threshold θ^- is set to the resting potential and θ^+ to the firing threshold of the AdEx model, i. e. $\theta^- = -70.6 \,\mathrm{mV}$ and $\theta^+ = -45.3 \,\mathrm{mV}$. The remaining five parameters τ_x , τ_- , τ_+ , $A_{\rm LTD}$ and $A_{\rm LTP}$ are fitted to each data set individually by the following procedure. We calculate the theoretically predicted weight change $\Delta w_i^{\mathrm{th},j}$ by integrating (analytically or numerically) Eq. (3), for a given experimental protocol j, as a function of the free parameters. We then estimate the free parameters by minimizing the mean-square error E between the theoretical calculations and the experimental data $\Delta w_i^{\mathrm{exp},j}$:

$$E = \sum_{j} \left(\Delta w_i^{\text{th},j} - \Delta w_i^{\exp,j} \right)^2.$$

For the data set in hippocampus [15], we also fit the two parameters θ^- and θ^+ since completely different preparations and cell type were used. Moreover for this data set, the time constant τ_x is taken from physiological measurements given in [13] and fixed to the values of 16ms. The parameters for the various experiments are summarized in table 1B.

6.4 Protocols and mathematical methods

Voltage clamp experiment. (Fig. 1H) The postsynaptic membrane potential was switched in the simulations to a constant value u_{clamp} chosen from -80mV to 0mV while presynaptic fibers were stimulated with either 25 (blue line) or 100 pulses (red line) at 50Hz. Due to voltage clamping, the actual value of the voltage u itself and the low-pass filtered versions \bar{u} are constant and equal to u_{clamp} . Hence, the synaptic plasticity rule becomes $\frac{d}{dt}w_i = -A_{\text{LTD}} X_i(t) \left[u_{\text{clamp}} - \theta_-\right]_+ + A_{\text{LTP}} \bar{x}_i(t) \left[(u_{\text{clamp}} - \theta_-)(u_{\text{clamp}} - \theta_+)\right]_+$.

Frequency dependence experiment. (Fig. 2B) Presynaptic spikes in the simulation were paired with postsynaptic spikes that were either advanced by +10ms or delayed by -10ms with respect to the presynaptic spike. This pairing was repeated 5 times with different frequencies ranging from 0.1 to 50Hz. These 5 pairings were repeated 15 times at 0.1Hz. However, the 5 pairing at 0.1Hz were repeated only 10 times to mimic the experimental protocol [23].

Burst-timing-dependent plasticity. (Fig. 3A) The presynaptic spike is paired $\Delta t = +10$ ms before (or $\Delta t = -10$ ms after) 1, 2 or 3 postsynaptic spikes. The frequency of the burst is 50Hz. The neuron receives 60 pairings at a frequency of 0.1Hz. Fig. 3B: The presynaptic spike is paired with a burst of 3 action potentials ($\Delta t = +10$ ms and -10ms), while the burst frequency varies from 20 to 100Hz. Fig. 3C: A presynaptic spike is paired with a burst of 3 postsynaptic action potentials with burst frequency of 50Hz. The time Δt between the presynaptic spike and the first postsynaptic action potential varies from -80 to 40 ms. For a detailed description of the experiments see [35].

Poisson input for functional scenarios. (Fig. 4-7) Poisson inputs are used in all the following experiments. They are generated by a stochastic process where the spike is elicited with a stochastic intensity ν .

Relation between connectivity and coding: Toy model. (Fig. 4) Weights of ten all-to-all connected neurons are initialized at 1, bounded between 0 and 3. Weights evolve with the voltage-based rule with homeostasis (Eq. 3) for 100s. The model is compared to a canonical pair-based STDP model written as $\frac{d}{dt}w_i = -A_{\text{LTD}}^{\text{pair}} X_i \bar{y} + A_{\text{LTP}}^{\text{pair}} \bar{x}_i Y$, where Y is the postsynaptic spike train defined the same way as the presynaptic spike train X_i with a filter of the postsynaptic spikes \bar{y} similar to \bar{x}_i . The parameters are chosen $A_{\text{LTD}}^{\text{pair}} = A_{\text{LTP}}^{\text{pair}} = 1e^{-5}$ for the amplitudes and τ_x for the time constant of \bar{x}_i as well as for the time constant of the postsynaptic low-pass filter \bar{y} . Rate code: Neuron 1 fire at 2Hz, neuron 2 at 4Hz... neuron 10 at 20Hz

following a Poisson statistics, i.e. short current pulses are injected to make the neuron fire with Poisson statistics at this frequency. The neurons have different reference values from $u_{ref}^2 = 60$ to 600mV^2 . Temporal code: Neurons fire successively every 20ms, first neuron 1 fires then 20ms later neuron 2 then... 10 then 1 etc, in a loop. The neurons have a reference value set to $u_{ref}^2 = 60 \text{mV}^2$.

Rate coding in network simulation. (Fig. 5) Five hundred presynaptic Poisson neurons with firing rates $\nu_i^{\rm pre}$ ($1 \le i \le 500$) are connected to 10 postsynaptic excitatory neurons. The inputs rates $\nu_i^{\rm pre}$ follow a Gaussian profile, i. e. $\nu_i^{\rm pre} = A \cdot \exp(-(i-\mu)^2/(2\sigma^2))$, with variance $\sigma = 10$ and amplitude A = 30Hz. The center μ of the Gaussian shifts randomly every 100ms between 10 different positions equally distributed. Circular boundary conditions are assumed, i.e. neuron i = 500 is considered as neighbor of i = 1. Synaptic weights of the feedforward connections are initialized randomly (uniformly in [0.5,2]) and hard bound are set to 0 and 3. The 10 excitatory neurons are all to all recurrently connected with a starting synaptic weight of 0.25 (hard bounds set to 0 and 0.75). In addition, 3 inhibitory neurons are randomly driven by 8 excitatory neurons and project on 6 excitatory neurons, also chosen randomly. Those random connections are fixed and have a weight equal to 1. The reference value is set to $u_{ref}^2 = 60 \text{mV}^2$ and the simulation time to 1000s. Parameters are normally chosen as in table 1B, visual cortex data, except for Fig. 5 B-E, where A_{LTP} and A_{LTD} where reduced by a factor 100.

Temporal coding in network simulation. (Fig. 6) Same setting than rate code but the patterns are presented for 20ms successively (from center position 500, to 450, to 400 etc in a circular manner). The reference value has been set to $u_{ref}^2 = 80 \text{mV}^2$.

ICA-like computation - Orientation selectivity with natural images. (Fig. 7) Ten natural images have been taken from the benchmark of Olshausen et al. [40]. A small patch of 16 by 16 pixels from any of the images is randomly chosen every 200ms. After prewhitening, the inputs for the "ON" ("OFF") image are Poisson spike trains generated by the positive (negative) part of the patch (with respect to a reference grey value reflecting the ensemble mean) with maximum frequency of 50Hz. The 2x16x16 inputs are connected to one postsynaptic neuron. The initial weights are set randomly between 0 and 2 and hard bounds are set between 0 and 3. The connections follow the synaptic rule (Eq. 3), where the reference value is set to $u_{ref}^2 = 50 \text{mV}^2$. Parameters are chosen as in table 1B (visual cortex data) but A_{LTP} and A_{LTD} where reduced by a factor 10. Every 20 s an extra normalization is applied to equalize the norm of the "ON" weights to the one of the "OFF" weights [31].

References

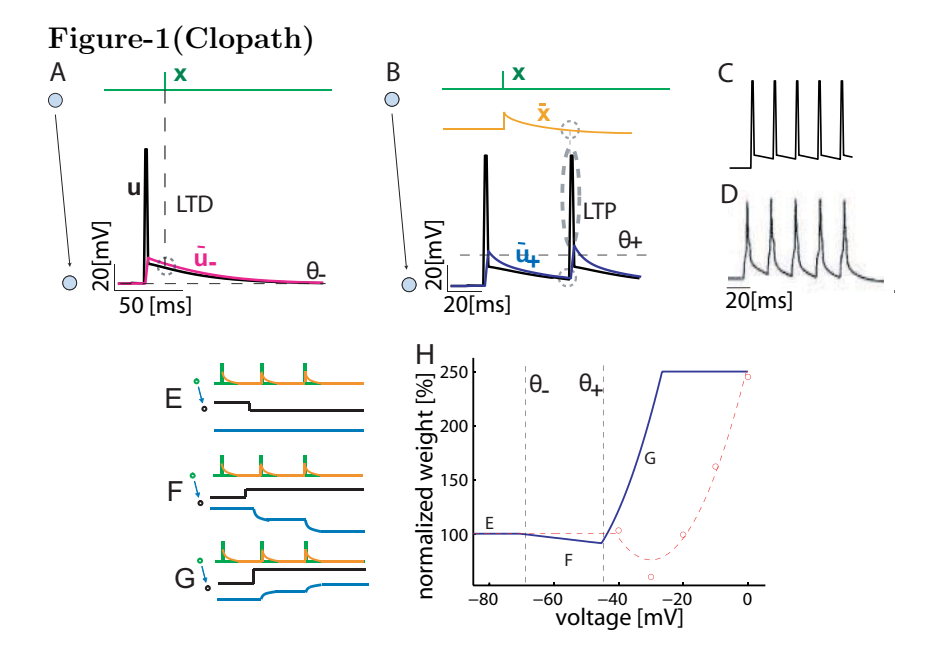
 D.V Buonomano and M.M. Merzenich. Cortical plasticity: From synapses to maps. Annual Review of Neuroscience, 21:149–186, 1998.

- [2] Y. Fregnac and D. Shulz. Activity-dependent regulation of receptive field properties of cat area 17 by supervised hebbian learning. J. Neurobiol, 41:69–82, 1999.
- [3] Robert C. Froemke, Michael M. Merzenich, and Christoph E. Schreiner. A synaptic memory trace for cortical receptive field plasticity. *Nature*, 450:425–429, 2007.
- [4] G. H. Recanzone, C. E. Schreiner, and M. M. Merzenich. Plasticity in the frequency representation of primary auditory cortex following discrimination training in adult owl monkeys. The Journal of Neuroscience, 13:87–103, 1993.
- [5] S. Song, P.J. Sjöström, M. Reigl, S. Nelson, and D.B. Chklovskii. Highly nonrandom features of synaptic connectivity in local cortical circuits. *PLoS Biology*, 3:507–519, 2005.
- [6] S. Lefort, C. Tomm, J.C.F. Sarria, and C.C.H. Petersen. The excitatory neuronal network of the c2 barrel column in mouse primary somatosensory cortex. *Neuron*, 61:301–316, 2009.
- [7] W Denk and H Horstmann. Serial block-face scanning electron microscopy to reconstruct three-dimensional tissue nanostructure. PLoS Biol, 2(11):e329. doi:10.1371/journal.pbio.0020329, 2004.
- [8] R. Yuste and T. Bonhoeffer. Genesis of dendritic spines: insights from ultrastructural and imaging studies. Nat Rev Neurosci, 5(1):24-34, 2004.
- [9] J. T. Trachtenberg, B. E. Chen, G. W. Knott, G. Feng, J. R. Sanes, E. Welker, and K. Svoboda. Long-term in vivo imaging of experience-dependent synaptic plasticity in adult cortex. *Nature*, 420:788–794, 2002.
- [10] D. O. Hebb. The Organization of Behavior. Wiley, New York, 1949.
- [11] Robert C. Malenka and Mark F. Bear. LTP and LTD: An embarassment of riches. Neuron, 44:5–21, 2004.
- [12] H. Markram, J. Lübke, M. Frotscher, and B. Sakmann. Regulation of synaptic efficacy by coincidence of postysnaptic AP and EPSP. Science, 275:213–215, 1997.
- [13] G.-q. Bi and M.-m. Poo. Synaptic modification of correlated activity: Hebb's postulate revisited. Ann. Rev. Neurosci., 24:139–166, 2001.
- [14] A. Artola, S. Bröcher, and W. Singer. Different voltage dependent thresholds for inducing long-term depression and long-term potentiation in slices of rat visual cortex. *Nature*, 347:69–72, 1990.
- [15] A. Ngezahayo, M. Schachner, and A. Artola. Synaptic activation modulates the induction of bidirectional synaptic changes in adult mouse hippocamus. J. Neuroscience, 20:2451–2458, 2000.
- [16] S. M. Dudek and M. F. Bear. Bidirectional long-term modification of synaptic effectiveness in the adult and immature hippocampus. J. Neuroscience, 13:2910–2918, 1993.
- [17] W. Gerstner, R. Kempter, J.L. van Hemmen, and H. Wagner. A neuronal learning rule for sub-millisecond temporal coding. *Nature*, 383(6595):76–78, 1996.

- [18] P.D. Roberts and C.C. Bell. Computational consequences of temporally asymmetric learning rules: II. Sensory image cancellation. Computational Neuroscience, 9:67–83, 2000.
- [19] R. Legenstein, C. Naeger, and W. Maass. What can a neuron learn with spike-timing dependent plasticity. Neural Computation, 17:2337–2382, 2005.
- [20] R. Guyonneau, R. VanRullen, and S.J. Thorpe. Neurons tune to the earliest spikes through stdp. Neural Computation, 17(4):859–879, 2005.
- [21] W. Gerstner and W. K. Kistler. Spiking Neuron Models. Cambridge University Press, Cambridge UK, 2002.
- [22] John Lisman and Nelson Spruston. Postsynaptic depolarization requirements for LTP and LTD: a critique of spike timing-dependent plasticity. Nature Neuroscience, 8(7):839–841, 2005.
- [23] P.J. Sjöström, G.G. Turrigiano, and S.B. Nelson. Rate, timing, and cooperativity jointly determine cortical synaptic plasticity. Neuron, 32:1149–1164, 2001.
- [24] H. Z. Shouval, M. F. Bear, and L. N. Cooper. A unified model of nmda receptor dependent bidirectional synaptic plasticity. Proc. Natl. Acad. Sci. USA, 99:10831–10836, 2002.
- [25] J.E. Lisman and A.M. Zhabotinsky. A model of synaptic memory: A CaMKII/PP1 switch that potentiates transmission by organizing an AMPA receptor anchoring assembly. Neuron, 31:191–201, 2001.
- [26] S. Song and L. F. Abbott. Cortical development and remapping through spike timing-dependent plasticity. Neuron, 32:339–350, 2001.
- [27] E. V. Lubenov and A. G. Siapas. Decoupling through synchrony in neuronal circuits with propagation delays. *Neuron*, 58:118–131, 2008.
- [28] A. Morrison, A. Aertsen, and M. Diesmann. Spike-timing dependent plasticity in balanced random networks. Neural Computation, 19:1437–1467, 2007.
- [29] Eugene M. Izhikevich and Gerald M. Edelman. Large-scale model of mammalian thalamocortical systems. Proceedings of the National Academy of Sciences, 105:3593–3598, 2008.
- [30] L.N. Cooper, N. Intrator, B.S. Blais, and H. Z. Shouval. Theory of cortical plasticity. World Scientific, Singapore, 2004.
- [31] K. D. Miller. A model for the development of simple cell receptive fields and the ordered arrangement of orientation columns through activity dependent competition between ON- and OFF-center inputs. J. Neurosci., 14:409–441, 1994.
- [32] J. P. Pfister and W. Gerstner. Triplets of spikes in a model of spike timing-dependent plasticity. J. Neursci., 26:9673–9682, 2007.

- [33] D.H. O'Connor, G.M. Wittenberg, and S.S.H. Wang. Dissection of Bidirectional Synaptic Plasticity Into Saturable Unidirectional Processes. *Journal of Neurophysiology*, 94:1565–1573, 2005.
- [34] G.G. Turrigiano and S.B. Nelson. Homeostatic plasticity in the developing nervous system. Nature Reviews Neuroscience, 5:97–107, 2004.
- [35] Thomas Nevian and Bert Sakmann. Spine ca2+ signaling in spike-timing-dependent plasticity. *J. Neurosci.*, 26(43):11001–11013, 2006.
- [36] J. Kozloski and G. A. Cecchi. Topological effects of spike timing-dependent plasticity. arxiv.org, abs:0810.0029, 2008.
- [37] S. P. Jadhav, J. Wolfe, and D. E. Feldman. Sparse temporal coding of elementary tactile features during active whisker sensation. *Nature Neuroscience*, page doi:10.1038/nn.2328, 2009.
- [38] J. J. Hopfield. Neural networks and physical systems with emergent collective computational abilities. Proc. Natl. Acad. Sci. USA, 79:2554–2558, 1982.
- [39] B. Blais, H. Shouval, and L. Cooper. Receptive field formation in natural scene environments: comparison of single-cell learning rules. *Neural Computation*, 10:1797–1813, 1998.
- [40] B. A. Olshausen and D. J. Field. Emergence of simple-cell receptive field properties by learning a sparse code for natural images. *Nature*, 381:607–609, 1996.
- [41] S. Martinez-Conde, S. Macknik, and D. Hubel. The role of fixational eye movements in visual perception. Nature Reviews Neuroscience, 5:229–240, 2004.
- [42] E. Oja. A simplified neuron model as a principal component analyzer. J. Mathematical Biology, 15:267–273, 1982.
- [43] A. Hyvaerinen, J. Karhunen, and E. Oja. Independent Component Analysis. Wiley-Interscience, 2001.
- [44] H.-X. Wang, R.C. Gerkin, D.W. Nauen, and G.-Q. Wang. Coactivation and timing-dependent integration of synaptic potentiation and depression. *Nature Neuroscience*, 8:187–193, 2005.
- [45] A. Saudargiene, B. Porr, and F. Wörgötter. How the shape of pre- and postsynaptic signals can influence stdp: A biophysical model. Neural Computation, 16:595–626, 2003.
- [46] J.M. Brader, W. Senn, and S. Fusi. Learning real-world stimuli in a neural network with spike-driven synaptic dynamics. *Neural Computation*, 19:2881–2912, 2007.
- [47] Claudia Clopath, Lorric Ziegler, Eleni Vasilaki, Lars Bsing, and Wulfram Gerstner. Tag-trigger-consolidation: A model of early and late long-term-potentiation and depression. PLoS Comput Biol, 4(12), Dec 2008.

- [48] P.J. Sjöström and M. Häusser. A Cooperative Switch Determines the Sign of Synaptic Plasticity in Distal Dendrites of Neocortical Pyramidal Neurons. Neuron, 51(2):227–238, 2006.
- [49] M. Tsodyks and H. Markram. The neural code between neocortical pyramidal neurons depends on neurotransmitter release probability. Proc. Natl. Academy of Sci., USA, 94:719–723, 1997.
- [50] U. Frey and R.G.M. Morris. Synaptic tagging and long-term potentiation. Nature, 385:533 536, 1997.
- [51] A.B. Barrett, G.O. Billings, R.G.M. Morris, and M.C.W. van Rossum. State based model of long-term potentiation and synaptic tagging and capture. *Plos Comp Biol*, 5(1):e1000259. doi:10.1371/journal.pcbi.1000259, 2009.
- [52] JM. Bekkers and M. Häusser. Targeted dendrotomy reveals active and passive contributions of the dendritic tree to synaptic integration and neuronal output. Proc. Natl. Acad. Sci. USA, 104(27):11447–11452, 2007.
- [53] R. Brette and W. Gerstner. Adaptive exponential integrate-and-fire model as an effective description of neuronal activity. J. Neurophysiol., 94:3637 – 3642, 2005.
- [54] L Badel, S Lefort, R Brette, CC Petersen, W Gerstner, and MJ Richardson. Dynamic i-v curves are reliable predictors of naturalistic pyramidal-neuron voltage traces. J Neurophysiol, 99:656 – 666, 2008.
- [55] E.M. Izhikevich. Which model to use for cortical spiking neurons? IEEE Transactions on Neural Networks, 15:1063–1070, 2004.
- [56] P.J. Sjöström, G.G. Turrigiano, and S.B. Nelson. Endocannabinoid-dependent neocortical layer-5 ltd in the absence of postsynaptic spiking. J. Neurophysiol., 92:3338–3343, 2004.



voltage[mV] voltage[mV] time [ms] voltage[mV] time [ms]	Figure-2(Clopath) A normalized weight[%] 140 normalized weight 120 normalized meight 12
voltage[mV] normalized weight [%] 0.1Hz + Dep 1.Hz + Dep 1.Hz + Dep 4.0Hz + Hyp 4.0Hz	normalized weight [%] ID

Figure-3(Clopath)

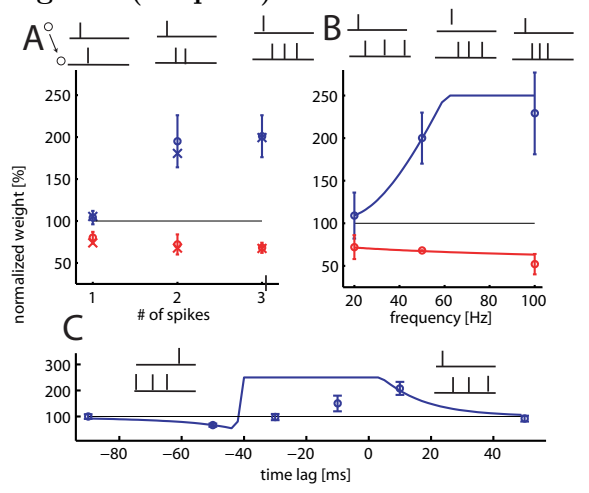


Figure-4(Clopath) A Rate Code B Temporal Code 36Hz 40Hz after before after neuron index neuron index 10 10 4 6 8 neuron index 4 6 8 neuron index \mathbf{C} D neuron index neuron index 8 10 10

4 6 8 neuron index

4 6 8 neuron index

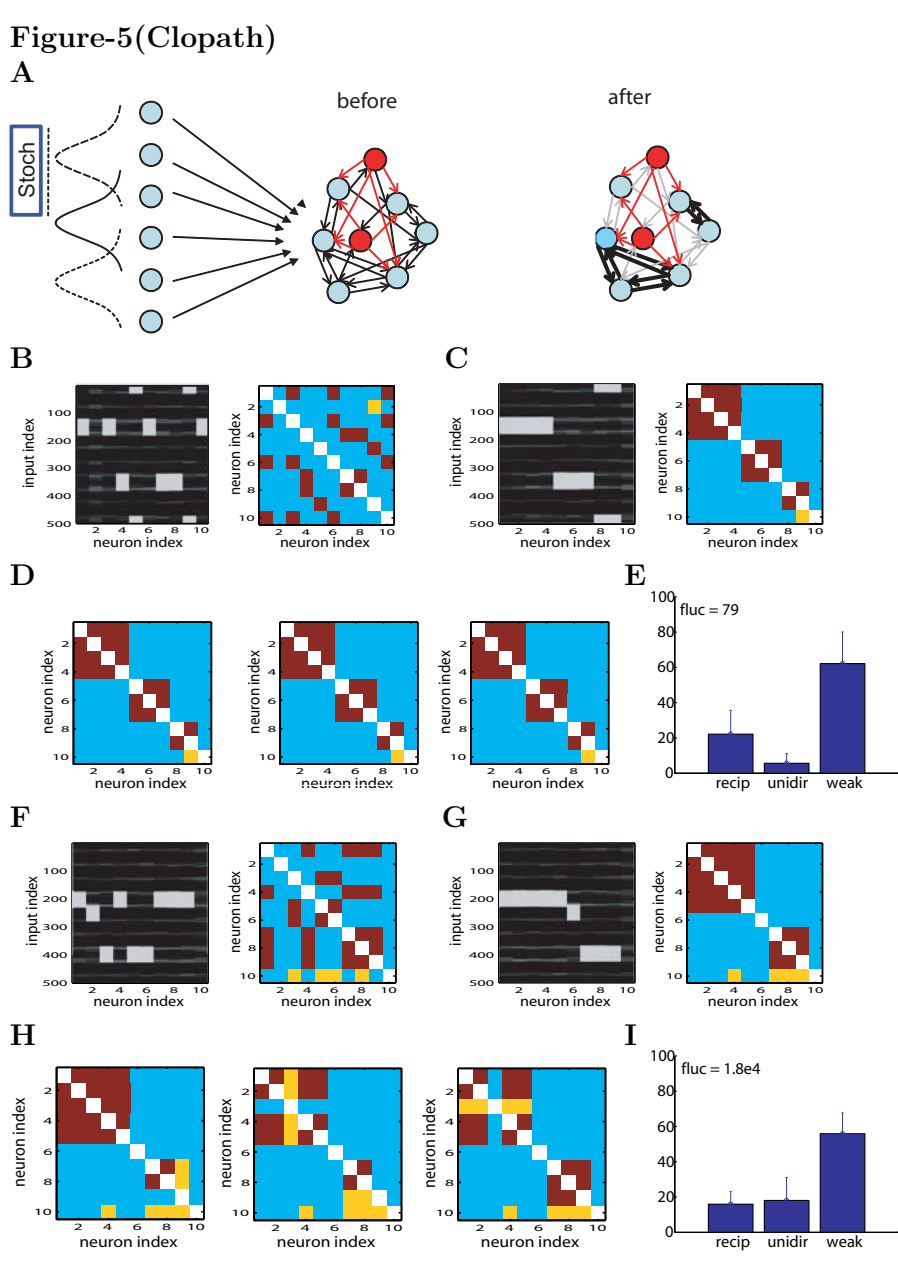


Figure-6(Clopath)

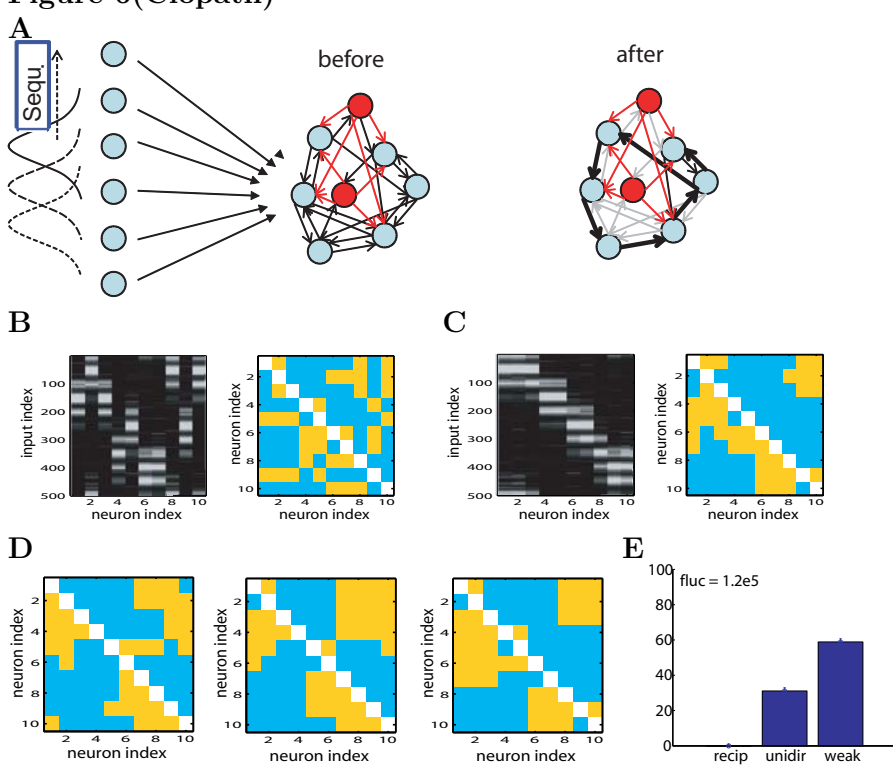


Figure-7(Clopath) A B ON Filter Filter OFF" weights

\mathbf{A}

Parameters	Value	
C - membrane capacitance	281pF	
g_L - leak conductance	$30 \mathrm{nS}$	
E_L - resting potential	$-70.6 \mathrm{mV}$	
Δ_T - slope factor	$2 \mathrm{mV}$	
$V_{T_{rest}}$ - threshold potential at rest	$-50.4 \mathrm{mV}$	
$ au_{w_{ad}}$ - adaptation time constant	144ms	
a - subthreshold adaptation	4nS	
b - spike triggered adaptation	80.5 pA	
I_{sp} - spike current after a spike	400nA	
τ_z - spike current time constant	$40 \mathrm{ms}$	
$ au_{V_T}$ - threshold potential time constant	$50 \mathrm{ms}$	
$V_{T_{max}}$ - threshold potential after a spike	-30.4mV	

 \mathbf{B}

Exper.	$\theta_{-}(mV)$	$\theta_+(mV)$	$A_{\rm LTD}(mV)^{-1}$	$A_{\rm LTP}(mV)^{-2}$	$\tau_x(ms)$	$\tau_{-}(ms)$	$\tau_+(ms)$
VC^*	-70.6	-45.3	$14\mathrm{e}^{-5}$	$8\mathrm{e}^{-5}$	15	10	7
SC	-70.6	-45.3	$21\mathrm{e}^{-5}$	$67\mathrm{e}^{-5}$	15	8	5
HP	-41	-38	$38\mathrm{e}^{-5}$	$2\mathrm{e}^{-5}$	16		